

1 **Flickering Gamma-Ray Flashes, the Missing Link between**
2 **Gamma Glows and TGFs**

3

4

5 N. Østgaard^{1*}, A. Mezentsev^{1***}, M. Marisaldi^{1,14***}, J. E. Grove², M. Quick³, H. Christian⁴, S.
6 Cummer⁵, M. Pazos⁶, Y. Pu⁵, M. Stanley⁷, D. Sarria¹, T. Lang³, C. Schultz³, R. Blakeslee³, I.
7 Adams⁸, R. Kroodsma⁸, G. Heymsfield⁸, N. Lehtinen¹, K. Ullaland¹, S. Yang¹, B. Hasan Qureshi¹,
8 J. Søndergaard¹, B. Husa¹, D. Walker⁴, D. Shy², M. Bateman⁴, P. Bitzer⁴, M. Fullekrug⁹, M.
9 Cohen¹⁰, J. Montanya¹¹, C. Younes¹², O. van der Velde¹¹, P. Krehbiel⁷, J. A. Roncancio¹¹, J. A.
10 Lopez¹¹, M. Urbani¹¹, A. Santos¹², D. Mach¹³

11

12

¹ Department of Physics and Technology, University of Bergen, Norway

² U.S. Naval Research Laboratory, Washington DC, USA

³ NASA Marshall Space Flight Center, Huntsville, USA

⁴ Department of Atmospheric Science, Earth System Science Center, University of Alabama in
Huntsville, USA

⁵ Duke University, USA

⁶ Instituto de Ciencias de la Atmosfera y Cambio Climatico, UNAM, Mexico

⁷ New Mexico Institute of Mining and Technology, USA

⁸ NASA Goddard Space Flight Center, Greenbelt, USA.

⁹ University of Bath, UK

¹⁰ Georgia Institute of Technology, USA

¹¹ Polytechnic University of Catalonia, Spain

¹² Universidad Nacional de Colombia, Columbia

¹³ Universities Space Research Association, Huntsville, Alabama, USA

¹⁴ Astrophysics and Space Science Observatory, National Institute for Astrophysics, Bologna,
Italy.

29

30

31

32

33

34

35

36

37

38

39

40

*E-mail: Nikolai.Ostgaard@uib.no, orcid.org/0000-0002-2572-7033

**E-mail: Andrey.Mezentsev@uib.no, orcid.org/0000-0002-3471-7267

***E-mail: Martino.Marisaldi@uib.no, orcid.org/0000-0002-4000-3789

44

45

46

47

48
49 Two different hard radiation phenomena are known to originate from
50 thunderclouds: Terrestrial Gamma-ray Flashes (TGFs)¹ and gamma-ray glows².
51 Both involve avalanche of electrons accelerated to relativistic energies, but are
52 different phenomena. Glows are known to last for one-to-hundreds of seconds, have
53 moderate intensities and originate from quasi-stationary thundercloud fields²⁻⁵.
54 TGFs exhibit high intensities and have characteristic durations of tens-to-hundreds
55 of microseconds⁶⁻⁹. TGFs often show close association with emission of strong radio
56 signals¹⁰⁻¹⁷ and optical pulses¹⁸⁻²¹ indicating involvement of lightning leaders in their
57 generation.
58

59 Here we report unique observations of a different phenomenon, which we call
60 Flickering Gamma-ray Flashes (FGFs). FGFs resemble usual multi-pulse TGFs²²⁻²⁴,
61 but with larger number of pulses and each pulse has a longer duration than ordinary
62 TGFs. FGF durations span from 20 to 250 milliseconds, which reaches the lower
63 boundary of the gamma-ray glow duration. FGFs are radio and optically silent,
64 which makes them distinct from normal TGFs. An FGF starts as an ordinary
65 gamma-ray glow, then suddenly increases exponentially in intensity, and turns into
66 an unstable, “flickering” mode with a sequence of pulses. FGFs could be the missing
67 link between the gamma-ray glows and conventional TGFs, whose absence has been
68 puzzling atmospheric electricity community for two decades.
69
70

71
72 The unexpected detection of this remarkable class of gamma-ray event, Flickering
73 Gamma-ray-Flashes (FGFs), was obtained during the ALOFT* aircraft campaign flying
74 at 20 km altitude over thunderstorms in Caribbean and Central America in July 2023.
75 For ALOFT, a NASA high-altitude aircraft was outfitted with an array of gamma-ray,
76 optical, radio, and electric field instruments designed to study energetic emissions and
77 lightning processes in thunderstorms (see Methods 2a).
78

79 One of two bright FGFs that was observed while passing over a gamma-glowing
80 thundercloud²⁵ off the western coast of El Salvador is shown in Fig. 1A. This FGF has
81 17 pulses, of which 8 pulses (#2-9) are so bright that the large Bismuth-Germanate
82 (BGO) gamma detector (225 cm^2) experienced saturation (Fig. 1A, inset), while the
83 Lutetium Yttrium Orthosilicate (LYSO) detector (Fig. 1A, inset) was not saturated due
84 to its much smaller detector area (1 cm^2) (see Methods 2a and 2b). The high fluence
85 observed in both BGO and LYSO indicates clearly that the source radial distance to the
86 foot-point was within 5 km range (see Methods 2a, 2e and 2f). The first pulses have
87 durations and interpulse times of several milliseconds, then the intensity of the pulses
88 increases and their duration decreases (down to 1-2 ms) until the pulse intensity
89 decreases and separation between pulses becomes larger (up to 20 ms). The total
90 duration of the FGF shown in Fig. 1 is ~50 ms.
91

* ALOFT: Airborne Lightning Observatory for FEGS and TGFs; FEGS: Fly’s Eye GLM Simulator;
GLM: Geostationary Lightning Mapper.

92 The Fly's Eye GLM Simulator (FEGS) onboard the aircraft did not show any optical
93 signals of 337 nm and 777 nm emissions, related to streamers and leaders, (see Methods
94 2d) during the pulses of the FGF (Fig. 1B). The FEGS field-of-view (FOV) is 10 km x
95 10 km** square, significantly smaller than the UIB-BGO FOV, which is circular with
96 ~20 km radius (see Methods 2a), but in this case the FGF source is well within the
97 FEGS FOV (see Methods 2e).

98

99 The Electric Field Change Meter (EFCM) also on board the aircraft, which records
100 close range Low Frequency (LF) electric field variations, shows no detectable
101 signatures of electric activity during the pulses but a rather strong Narrow Bipolar Event
102 (NBE) occurred 9 ms after the last pulse, followed by continuous lightning activity, as
103 seen in both radio and optical data (Fig. 1B and Methods: Extended Data Fig. 1 and 4).

104

105 The ground-based LF radio data from the closest campaign radio receiver in Sisal,
106 Mexico, 920 km away is shown in Fig. 1C and confirms that no radio signals that can be
107 associated with the FGF pulses are seen, including the first few FGF pulses not captured
108 by the EFCM. From this range, the background noise is equivalent in amplitude to
109 lightning signals of very weak 1 kA peak current (see Methods 2c and Extended Data
110 Fig. 2). Although there are numerous lightning pulses in the data window shown, most
111 arrive at the sensor from a different direction than the known direction to the ER-2. The
112 two axis orthogonal measurements are rotated so that a signal originating from that
113 direction will have a large azimuthal B_ϕ (blue curve) component and a negligible radial
114 B_r (red curve) component. The pulse at 12.474 seconds has a large B_r component and
115 originates from a lightning source 725 km west of the ER-2 according to the Global
116 Lightning Detection Network (GLD360). The NBE seen by EFCM was also seen in LF
117 in Mexico (Fig. 1C).

118

119 Twenty-four FGFs were observed during five of ten total flights, each of which spent 2-
120 3 hours above active gamma-glowing thunderclouds²⁵. Fig. 2 shows all the FGFs
121 observed by the BGO detectors, with the in-Situ Thunderstorm Observer for Radiation
122 Mechanisms (iSTORM) data overlaid for 21 of them. The count rates measured by
123 iSTORM are about $\frac{1}{2}$ to $\frac{2}{3}$ of what BGO measures, consistent with the smaller detector
124 geometric area (157 cm^2 versus 225 cm^2) and the smaller energy range (up to 5 MeV
125 versus 30 MeV). The iSTORM data acquisition system is fully independent from that of
126 the BGO. Despite some small differences (see Methods 2b), the two independent
127 detector systems confirm that the FGF is a real phenomenon and cannot be a result of
128 instrumental effects.

129

130 The FGFs were observed east of Yucatan, on the western coast of El Salvador, the coast
131 of the Mexican states of Tabasco and Veracruz and on the east coast of Florida. All
132 FGFs were observed over coastal regions and above gamma-glowing thunderclouds.
133 The typical duration of the pulses is 1-2 millisecond, separated by 1-20 milliseconds,
134 with the whole FGF lasting for tens to several hundreds of milliseconds. The FGFs
135 typically start with a couple of less intense but longer (5-20 ms) pulses. Then a train of
136 shorter (0.4-4 ms) intense pulses follows. Towards the end of the FGF the pulse
137 intensity decreases and the separation between pulses becomes larger.

138

** +/- 5 km times +/- 5km from aircraft foot-point for cloud top at 15 km.

139 We have LF radio recordings for all 24 FGFs, EFCM for 3 of them, and optical data for
140 22 FGFs, and no detectable radio signals or optical pulses that could be associated with
141 the pulses of the FGFs were observed. According to our observations, FGFs are both
142 radio and optically silent (see Methods 2c and 2d), in contrast to normal lightning-
143 related TGFs.

144
145 Multi-TGFs with a few pulses and associated radio signals have been observed by
146 several spacecraft²²⁻²⁴, but only CGRO/BATSE^{*1} with its very large detector area
147 (16000 cm^2) observed multi-TGFs that resemble the FGFs we report here. At the time
148 they were identified and explained as just an atypical form of lightning-related TGFs¹,
149²⁶. There have been a few modelling efforts that managed to reproduce the main features
150 of the multi-TGFs observed by CGRO/BATSE²⁷⁻²⁸. In these models the multi-TGF is
151 initiated by a lightning discharge and should be accompanied by significant charge
152 moment changes and strong currents²⁷⁻²⁸. None of these features was observed during
153 the FGFs we report here. Our observations show very clearly that there are no
154 detectable radio signals, even when we are only 5-10 km away from the source, and
155 there is no optical signal from any lightning leader, as should have been seen in the 777
156 nm and 337 nm bands.
157

158 Another remarkable feature is that in 17 of the 24 observations, the FGF was followed
159 by an NBE, not immediately (microseconds) after²⁸, but a few to tens of milliseconds
160 after the last observed FGF pulse, followed by continuous lightning activity for
161 hundreds of milliseconds, as seen in both radio and optical data (see Methods 2c and 2d
162 and Extended Data Fig. 1 and 4). This raises the intriguing possibility that gamma-ray
163 generation by thunderstorms, in the form of FGFs, plays a role at least in some lightning
164 initiation, which is a process that remains at best poorly understood.
165

166 During the ten flights of the campaign, we observed a total of 130 transient gamma-ray
167 events: 24 FGFs, 96 TGFs and 10 glow bursts (< 100 ms)²⁵. All of the TGFs and FGFs
168 were observed when passing over gamma-glowing thunderclouds. Only a few of the
169 TGFs (3 or 4) had intensities bright enough to be seen from space, which means that, at
170 least in the Caribbean and Central America during summer, the thunderclouds produce
171 almost 2 orders of magnitude more gamma flashes than can be detected from space and
172 which questions the “rarity” of TGFs²⁹⁻³⁰. Our findings are broadly consistent with those
173 from the Telescope Array in Utah, which has found many weak downward TGFs
174 associated with cloud-to-ground lightning flash development, in showing that gamma-
175 ray generation from thunderstorms is much more common and takes many more forms
176 than we previously knew³¹.
177

178 Both TGFs and FGFs have a spectral shape that is expected from the Relativistic
179 Runaway Electron Avalanche (RREA) process (see Methods 2e). This means that both
180 phenomena require large potentials (hundreds of MV) and electric fields above the
181 RREA threshold (280 kV/m surface equivalent) over large distances to accelerate
182 electrons to relativistic energies and subsequently produce high energy gamma photons.
183 Our observations show that the continuous RREA spectra of the FGFs extend to at least
184 31 MeV. While the electrons in the TGFs are accelerated in the strong transient electric
185 fields associated with lightning¹⁰⁻¹⁴, the FGFs reported here are not associated with the
186 electric field of lightning discharges.
187

* CGRO/BATSE: Compton Gamma-Ray Observatory/ Burst And Transient Source Experiment

188 When optical measurements are available¹⁸⁻²¹, TGFs are always associated with optical
189 pulses simultaneous or slightly delayed to the TGF, while there are no optical pulses
190 associated with the FGFs, indicating that leaders are involved in the generation of TGFs
191 but not in FGFs. The TGFs also show close association with radio emissions¹⁰⁻¹⁷, while
192 there are no detectable radio signals (see Methods 2c) from FGFs. None of the FGFs are
193 accompanied by TGFs.

194

195 Compared to gamma-ray glows, which are also radio and optically silent, the FGFs have
196 much shorter duration and higher intensities. Similar to both TGFs and FGFs, the
197 spectrum from gamma-ray glows also has the shape expected from the RREA process³².
198 FGFs start as an ordinary gamma-ray glow, then experience sudden exponential
199 increase, and turns into an unstable, “flickering”, mode, falling into separate pulses.
200

201 Compared to TGFs the durations of the pulses in the FGFs are significantly longer (>1
202 ms) than that of the TGFs (~10-100 us)⁶⁻⁹. Scaling the flux values of TGFs seen from
203 space down to 20 km altitude, we find that the brightest pulse in an FGF is just below
204 the lower threshold that can be identified from space, consistent with the non-detection
205 of FGFs by current space borne instruments⁶⁻⁹ (see Methods 2e and 2f). The
206 comparative characteristics of gamma-ray glows, FGFs and TGFs are summarized in
207 Table 1.
208

209 Both observationally and phenomenologically the FGFs differ from both TGFs and
210 gamma-ray glows but carry features of both. Both in pulse duration and total duration
211 and intensities, the FGFs fill the gap in the distribution of gamma emission phenomena
212 from thunderclouds, between gamma-ray glows on one side and TGFs on the other side
213 (Table 1). We therefore suggest that they can be the missing link between the two
214 phenomena.
215
216
217
218
219
220
221
222
223
224
225
226
227
228
229
230
231
232
233
234
235
236
237
238
239

240

241 **References**

242

- 243 1 Fishman, G. J., Bhat, P. N., Mallozzi, R., Horack J. M., Koshut, J. M. et al. Discovery
 244 of Intense Gamma-Ray Flashes of Atmospheric Origin, *Science*, 264, 1313–1316,
 245 doi:10.1126/science.264.5163.1313 (1994).
- 246
- 247 2 Parks, G. K., Mauk, B. H., Spiger, R., & Chin, J. X-ray enhancements detected during
 248 thunderstorms and lightning activity. *Geophysical Research Letters*, 8(11), 1176–1179
 249 (1981).
- 250
- 251 3 Eack, K. B., Beasley, W. H., Rust, W. D., Marshall, T. C., & Stolzenburg, M. Initial
 252 results from simultaneous observation of X-rays and electric fields in a thunderstorm.
 253 *Journal of Geophysical Research*, 101(D23), 29,637–29,640 (1996).
- 254
- 255 4 Østgaard, N , Christian, H. J., Grove, J. E. , Sarria, D., A. Mezentsev, A., et al. Gamma-
 256 ray glow observations at 20 km altitude. *Journal of Geophysical Research*, doi:
 257 10.1029/2019JD030312, (2019).
- 258
- 259 5 Wada, Y., Matsumoto, T., Enoto, T., Nakazawa, K. , Yuasa, T., et al. Catalog of gamma-
 260 ray glows during four winter seasons in Japan. *Physical Review Research*, 3, 043117 doi:
 261 10.1103/PhysRevResearch.3.043117 (2021).
- 262
- 263 6 Smith, D. M., Lopez, L. I. , Lin, R. P. and Barrington-Leigh, C. P., Terrestrial gamma-
 264 ray flashes observed up to 20 MeV, *Science*, 307(5712), 1085–1088,
 265 doi:10.1126/science.1107466 (2005).
- 266
- 267 7 Marisaldi, M., Fuschino, F., Labanti, C., Galli, M., Longo, F., et al. Detection of
 268 terrestrial gamma ray flashes up to 40 MeV by the AGILE satellite. *Journal of*
 269 *Geophysical Research*, 107, A00E13. <https://doi.org/10.1029/2009JA014502> (2010).
- 270
- 271 8 Briggs, M. S., Fishman, G. J., Connaughton, V., Bhat, P. N., Paciesas, W. S., et al. First
 272 results on terrestrial gamma ray flashes from the Fermi Gamma-ray Burst Monitor.
 273 *Journal of Geophysical Research*, 115, A07323. <https://doi.org/10.1029/2009JA015242>
 274 (2010).
- 275
- 276 9 N. Østgaard, N., T. Neubert, T., V. Reglero, V., K. Ullaland, K., S. Yang, S., et al. First
 277 ten months of TGF observations by ASIM. *Journal of Geophysical Research*. doi:
 278 10.1029/2019JD031214, (2019).
- 279
- 280 10 Stanley, M. A., Shao, X.-M., Smith, D. M., Lopez, L. I., Pongratz, M. B., et al. A link
 281 between terrestrial gamma-ray flashes and intracloud lightning discharges. *Geophysical*
 282 *Research Letters*, 33, L06803. <https://doi.org/10.1029/2005GL025537> (2006)
- 283
- 284 11 Cummer, S. A., Zhai, Y., Hu, W., Smith, D. M., Lopez, L. I., & Stanley, M. A.
 285 Measurements and implications of the relationship between lightning and terrestrial
 286 gamma ray flashes. *Geophysical Research Letters*, 32, L08811.
 287 <https://doi.org/10.1029/2005GL022778> (2005).
- 288

- 289 12 Lu, G., Blakeslee, R. J., Li, J., Smith, D. M., Shao, X.-M., et al. Lightning mapping
290 observation of a terrestrial gamma-ray flash. *Geophysical Research Letters*, 37, L11806.
291 <https://doi.org/10.1029/2010GL043494> (2010)
- 292
- 293 13 Shao, X.-M., Jacobsen, A. R., & Fitzgerald, T. J. Radio frequency radiation beam
294 pattern of lightning return strokes: A revisit to theoretical analysis. *Journal of*
295 *Geophysical Research*, 109, D19108. <https://doi.org/10.1029/2004JD004612> (2004).
- 296
- 297 14 Cummer, S. A., Lu, G., Briggs, M. S., Connaughton, V., Xiong, S., Fishman, G. J., &
298 Dwyer, J. R. The lightning–TGF relationship on microsecond timescales. *Geophysical*
299 *Research Letters*, 38, L14810. <https://doi.org/10.1029/2011GL048099> (2011).
- 300
- 301 15 Connaughton, V., Briggs, M. S., Xiong, S., Dwyer, J. R., Hutchins, M. L., et al. Radio
302 signals from electron beams in terrestrial gamma ray flashes, *Journal of Geophysical*
303 *Research*, 118, doi:10.1029/2012JA018288 (2013).
- 304
- 305 16 Cummer, S. A., Lyu, F., Briggs, M. S., Fitzpatrick, G., Roberts, O. J., & Dwyer, J. R.
306 Lightning leader altitude progression in terrestrial gamma-ray flashes. *Geophysical*
307 *Research Letters*, 42, 7792–7798. <https://doi.org/10.1002/2015GL065228> (2015).
- 308
- 309 17 Dwyer, J. R., & Cummer, S. A. Radio emissions from terrestrial gamma-ray flashes.
310 *Journal of Geophysical Research*, 118, 3769–3790. <https://doi.org/10.1002/jgra.50188>
311 (2013).
- 312
- 313 18 Østgaard, N., Gjesteland, T., Carlson, B. E., Collier, A. B., Cummer, et al.
314 Simultaneous observations of optical lightning and terrestrial gamma ray flash from
315 space. *Geophysical Research Letters*, 40, 2423–2426. <https://doi.org/10.1002/grl.50466>
316 (2013).
- 317
- 318 19 Neubert, T., Østgaard, N., Reglero, V., Chanrion, O., Heumesser, et al. A terrestrial
319 gamma-ray flash and ionospheric ultraviolet emissions powered by lightning. *Science*,
320 367(6474), 183–186. <https://doi.org/10.1126/science.aax3872> (2020).
- 321
- 322 20 Østgaard, N., Cummer, S. A., Mezentsev, A., Luque, A., J. Dwyer, J., et al.
323 Simultaneous observations of EIP, TGF, Elve and optical lightnings. *Journal of*
324 *Geophysical Research*, doi: 10.1029/2020JD033921, (2021).
- 325
- 326 21 Skeie, C. A., Østgaard, N., Mezentsev, A., Bjørge-Engeland, I., Marisaldi, M. et al.
327 The temporal relationship between Terrestrial Gamma-ray flashes and associated optical
328 pulses from lightning. *Journal of Geophysical Research*, doi: 10.1029/2022JD037128,
329 (2022).
- 330
- 331 22 Mezentsev, A., Østgaard, N., Gjesteland, T., Albrechtsen, K., Marisaldi, M., et al.
332 Radio emissions from double RHESSI TGFs. *Journal of Geophysical Research*, doi:
333 10.1002/2016JD025111, (2016).
- 334
- 335 23 Stanbro, M. C., Briggs, M. S., Roberts, O. J., Cramer, E. S., Cummer, S. A., & Grove,
336 J. E. A study of consecutive terrestrial gamma-ray flashes using the Gamma-ray Burst
337 Monitor. *Journal of Geophysical Research*, 123, 9634–9651.
338 <https://doi.org/10.1029/2018JA025710> (2018).

- 339
340 24 Mailyan, B., Stanbro, M., Briggs, M. S., Cummer, S., Dwyer, et al. Radio frequency
341 emissions associated with multi-pulsed Terrestrial Gamma-ray Flashes. *Journal of*
342 *Geophysical Research*, 126, e2020JA027928. <https://doi.org/10.1029/2020JA027928>
343 (2021).
- 344
345 25 Marisaldi, M., Østgaard, N., Lang, T., Sarria D., Mezentsev, A., et al. Tropical
346 Thunderclouds Glow in Gamma Rays for Hours and over Thousands of Square
347 Kilometers, *Nature Letter*, this edition (2024)
- 348
349 26 Nemiroff, R. J., Bonnell, J. T., Norris, J. P. Temporal and spectral characteristics of
350 terrestrial gamma flashes, *Journal of Geophysical Research*, Vol. 102, No. A5, 9659-
351 9665 (1997).
- 352
353 27 Dwyer, J. R., The relativistic feedback discharge model of terrestrial gamma ray
354 flashes, *Journal of Geophysical Research*, 117, A02308, doi:10.1029/2011JA017160
355 (2012).
- 356
357 28 Liu, N. Y., and J. R. Dwyer, Modeling terrestrial gamma ray flashes produced by
358 relativistic feedback discharges, *Journal of Geophysical Research*, 118, 2359–2376,
359 doi:10.1002/jgra.50232 (2013).
- 360
361 29 Smith, D. M., Dwyer, J. R., Hazelton, B. J., Grefenstette, B. W., Martinez-McKinney, G. F.
362 M., et al. The rarity of terrestrial gamma-ray flashes, *Geophysical Research Letters*, 38,
363 L08807, doi:10.1029/2011GL046875 (2011).
- 364
365 30 Østgaard, N., Gjesteland, T., Hansen, R. S., Collier, A. B., Carlson, B. E. The true
366 fluence distribution of terrestrial gamma flashes at satellite altitude. *Journal of*
367 *Geophysical Research*, Vol. 117, A03327, doi:10.1029/2011JA017365, (2012).
- 368
369 31 Belz, J. W., Krehbiel, P. R., Remington, J., Stanley, M. A., Abbasi, R. U., LeVon, R.,
370 et al. Observations of the origin of downward terrestrial gamma-ray flashes. *Journal of*
371 *Geophysical Research*, 125, e2019JD031940, doi: [10.1029/2019JD031940](https://doi.org/10.1029/2019JD031940) (2020).
- 372
373 32 Sarria, D., Østgaard, N., Marisaldi, M., Lehtinen, N. G., Mezentsev, A., Library of
374 simulated gamma-ray glows and application to previous airborne observations
375 *Journal of Geophysical Research*, doi: 10.1029/2022JD037956, (2023).
- 376
377
378 **Acknowledgements:** This work made use of data from UIB-BGO, iSTORM, FEGR, EFCM, LF
379 and VHF, GLD360. The ALOFT campaign and the UIB-BGO instrument was supported by
380 European Research Council under the European Union's Seventh Framework Programme
381 (FP7/2007–2013)/ERC grant agreement no. 320839 and the Research Council of Norway under
382 contracts 223252/F50 (CoE) and contract 325582. Some of the simulations were performed on
383 resources provided by UNINETT Sigma2, the National Infrastructure for High Performance
384 Computing and Data Storage in Norway, under project no. NN9526K. Work at NRL on ALOFT
385 is supported by the Office of Naval Research 6.1 funds. In addition, D. Shy is supported by the
386 U.S. Naval Research Laboratory's Jerome and Isabella Karle Fellowship. The FEGR and EFCM
387 team acknowledge the work of Scott Podgorny, David Corredor, and Mike Stewart. S. Cummer
388 and Y. Pu were partly supported by the National Science Foundation Dynamic and Physical
389 Meteorology program through Grant AGS-2026304. The use of the VHF data was supported by

390 US NSF Grants 1720600 and 2214044. Arthur Freeman, Robert Bernath, April Lamoureux and
391 Robert Brown of the University of Central Florida assisted with the deployment and maintenance
392 of the VHF interferometer at the TISTEF site. Martin Fullekrug was sponsored by the Royal
393 Society (UK) grant NMG/R1/180252 and the Natural Environment Research Council (UK) under
394 grants NE/L012669 /1 and NE/H024921/1. Significant financial and logistical support for
395 ALOFT was provided by the NASA Earth Science Division. We thank the governments of
396 Mexico, Bahamas, Colombia, Belize, Guatemala, Honduras, Nicaragua, Panama, Dominican
397 Republic, Costa Rica, El Salvador, Haiti, Turks & Caicos, Jamaica, and the Cayman Islands for
398 approving ER-2 overflights in support of ALOFT. GOES MDS sectors in support of ALOFT were
399 enabled by NOAA. We want to thank the ER-2 Project Team at NASA Armstrong Flight
400 Research Center, and the MacDill Air Force Base for hosting.

401

402 **Author Contributions:** N.O. and A.M. have led this study. The ALOFT campaign was led by
403 N.O., T.L. M.M. and C.S. The UIB-BGO instrument was provided by N.O., M.M., K.U., S.Y.
404 B.H.Q, J. S and B. H. and analyzed by N.O., M.M., D.S., N.L. The iSTORM data were provided
405 and analyzed by J.E.G., D.S. and D. W. The FEGS data were provided by M.Q and the EFCM
406 data were provided by H.C. and R. B. Radio data used in this study were provided and analyzed
407 by S.C., Y.P. and M.P. and other LF stations were operated by P.B., M.F., M.C., J.M, C.Y.,
408 O.vdV. J.A.R, J.A.L., M.U. and A.S. The VHF data were provided and analyzed by M.S. and P.K.
409 Radar data for the entire campaign were provided by I.A., R.K. and G.H.

410

411 **Competing Interests:** The authors declare that they have no competing financial interests.

412

413 **Correspondence** Correspondence and requests for materials should be addressed to N. Østgaard
414 (Nikolai.Ostgaard@uib.no), A. Mezentsev (Andrey.Mezentsev@uib.no), and M. Marisaldi
415 (Martino.Marisaldi@uib.no).

416

417

418

419

420

421

422

423

424

425

426

427

428

429

430

431

432

433

434

435

436

437

438

439

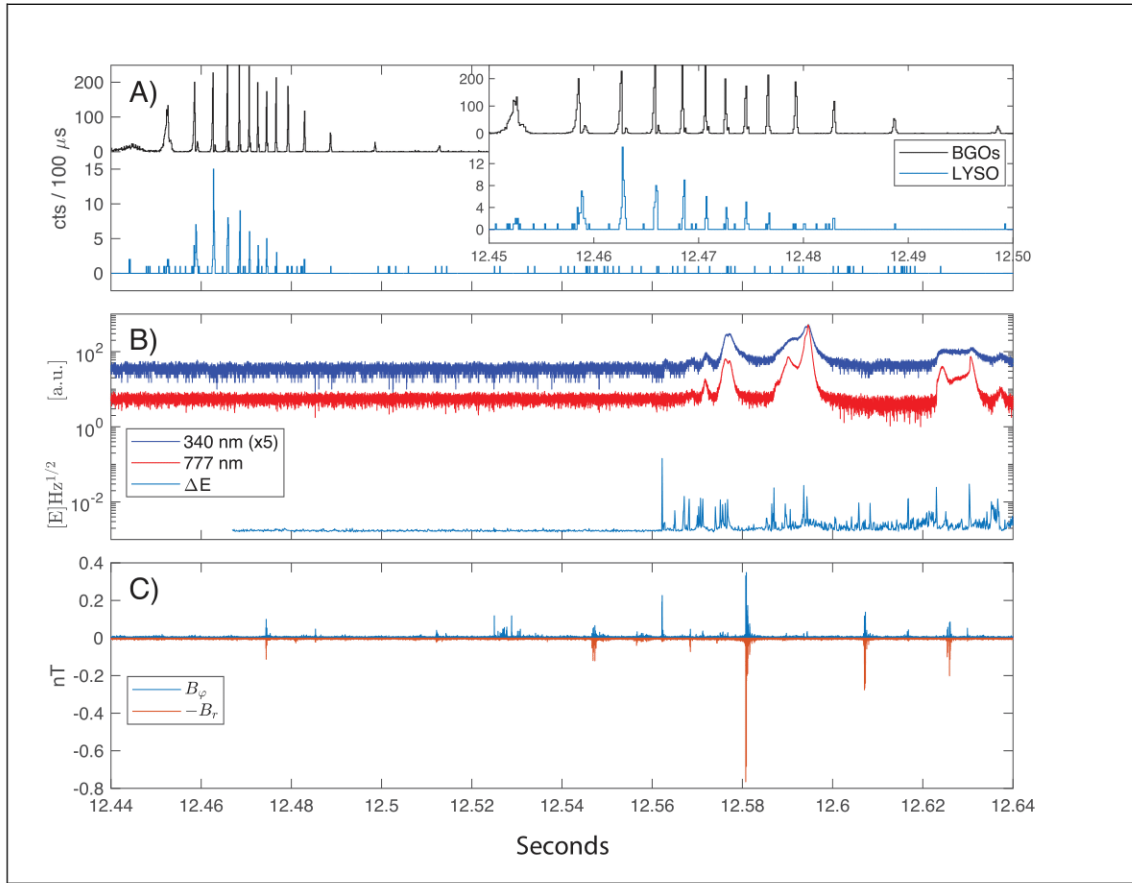
440

441

442

443
444
445
446
447
448

FIGURES AND TABLES



449
450
451
452
453
454
455
456

Fig. 1. Flickering Gamma-ray Flashes: 08.07. 2023: 05:01:12.44 UT - 05:01:12.64 UT. A) Gamma emissons measured by BGO and LYSO. The inset is zoomed in on the FGF time interval. B) FEGR optical emissions: 777 nm (red), 337 nm (blue) and EFCM: Electric field variability (ΔE), C) Low Frequency magnetic field radio emissions from Sisal, Mexico: radial (B_r) and azimuthal (B_φ) components.

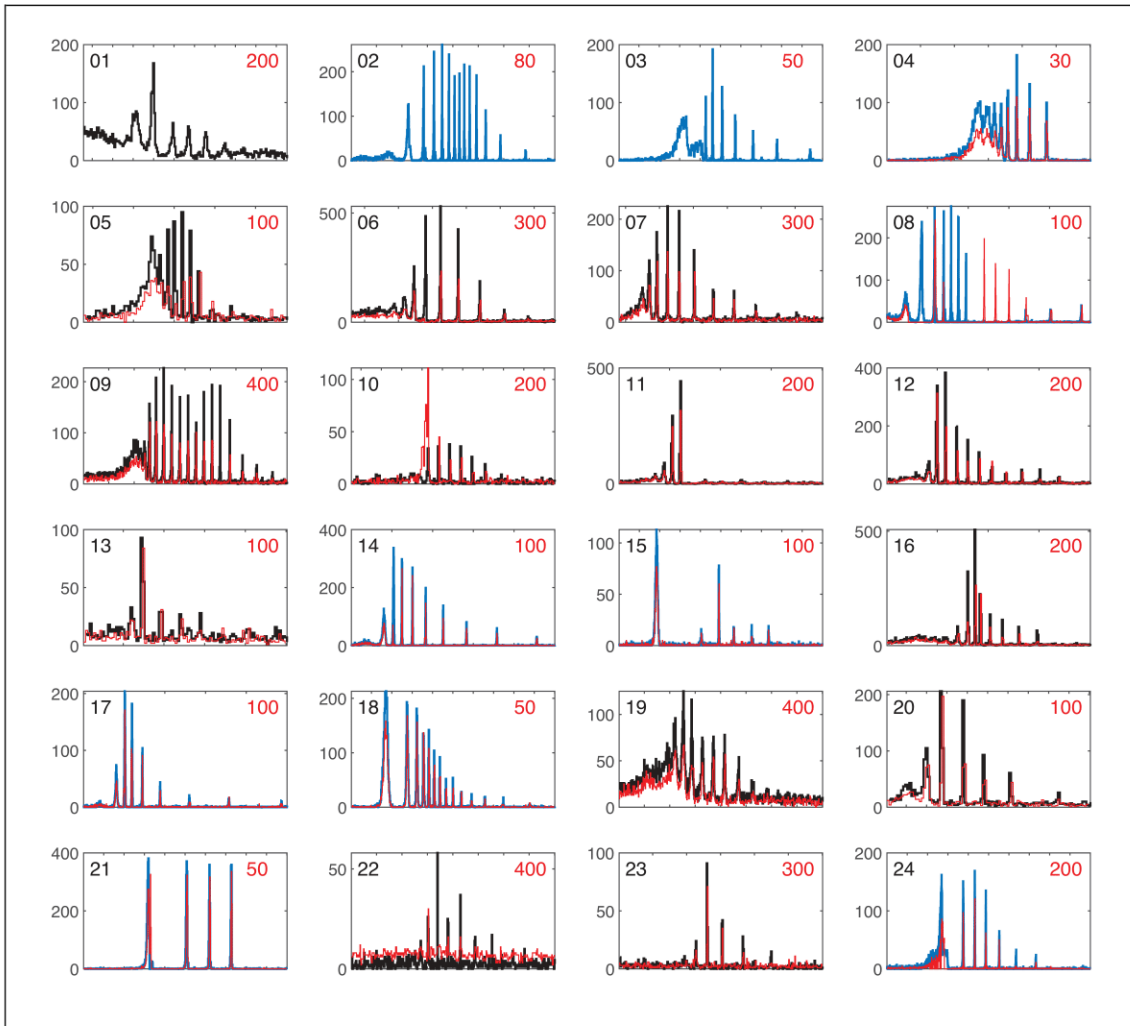


Fig. 2. Twenty-four FGFs seen by ALOFT. The BGO data are shown with black (cnts/1ms) and blue (cnts/100 μ s) and iSTORM data (for 21 of them) are overlaid in red with corresponding time bins. The values in the upper right corner (in red) are the time interval in millisecond shown in each plot. The numbering in the upper left corner is the event ID, which corresponds to dates and times of each event that are given in Extended Data Table 5.

Table 1. Characteristics of glows, FGFs and TGFs observed at 20 km altitude.

Event	Event duration	Peak flux (cm ⁻² s) ⁻¹	Optical	Radio	Spectra	Related to glows
Glow	1-100 s	¹ 2 -90	No	No	RREA ¹	Yes ¹
FGF total	10-100 ms	² 1.8 x 10 ² – 6.0 x 10 ⁴	No	No	RREA ¹	Yes ¹
TGF	10-1000 us	³ 5.6 x 10 ⁵ – 10 ⁸	Yes ⁴	Yes ⁵	RREA ¹	Yes ¹

¹ From the ALOFT campaign.

² Max peak flux in BGO of single pulse in a FGF, when saturation is accounted for (see Methods 2f).

³ ASIM TGFs mapped down to 20 km.

⁴ When optical measurements are available.

⁵ Some TGFs have no detectable radio.

476 **METHODS**

477

478 **1. THE CAMPAIGN – OVERVIEW AND MISSION STRATEGY**

479

480 During the month of July 2023 an aircraft campaign over thunderstorms in Caribbean
481 and Central America with the NASA ER-2 aircraft was conducted; Airborne Lightning
482 Observatory for FEGS* and TGFs (ALOFT). A total of ten flights (3-8 hours each) at 20
483 km altitude were performed. Each flight spent 3-4 hours above active thunderstorms.

484

485 The scientific target of the ALOFT campaign was to observe Terrestrial Gamma-ray
486 Flashes (TGF) and gamma-ray glows from thunderstorms and the possible connection
487 between the two. The aircraft was equipped with five independent gamma-ray detectors,
488 30 photometers, seven electric field sensors, two radars and two microwave radiometer
489 systems. In addition, we had nine ground-based radio receivers operated during the
490 campaign, covering Very Low Frequencies (VLF), Low Frequencies (LF) and two VHF
491 Interferometers. The instruments used in this study will be described below.

492

493 Taking advantage of the novel mission concept, where one-second resolution data were
494 downlinked in real-time, gamma-glowing clouds could be identified in real time, and
495 the pilot was instructed to return to the same location as long as the thundercloud was
496 glowing.

497

498 During these ten flights we observed a total of 130 transient gamma-ray events, 10 glow
499 bursts (< 100 ms)²⁵, 96 TGFs and 24 Flickering Gamma-ray Flashes (FGFs), which we
500 find to be a fundamentally different type of hard radiation from thunderclouds than the
501 TGFs.

502

503

504 **2. INSTRUMENTATION AND DATA ACQUISITION**

505

506 **a) Instrument description**

507

508 ***The Bismuth-Germanate instrument from the University of Bergen (UIB-BGO).***

509 This instrument had four independent gamma detectors; one BGO detector, with three
510 independent pairs of BGO scintillators read out by Photomultiplier Tubes (PMT) and
511 three Lutetium Yttrium Orthosilicate (LYSO) detectors, all with fast readout electronics
512 and with different geometric areas ranging from 0.09 cm² to 225 cm². From modelling
513 work³³ it was expected that the count rate could increase by 4 orders of magnitude,
514 depending on how close to the source the aircraft would be. Consequently, we designed
515 our detectors to cover 4 orders of magnitude in count rates. The geometric areas, energy
516 ranges and time resolutions for the four detectors are given in Extended Data Table 1.
517 The three BGO/PMT detectors are similar to one of the four High Energy Detector
518 modules of the Modular X- and Gamma-ray Sensor (MXGS)³⁴ that is flying on
519 Atmosphere Space Interaction Monitor (ASIM) on the International Space Station
520 (ISS). At 20 km altitude the BGO detectors are able to see events up to ~20 km radius
521 from the foot-point of the aircraft³³. The three BGO/PMT detectors and the medium
522 LYSO/PMT detector share the same read-out electronics, while the two other
523 LYSO/SiPM detectors have a separate read-out system.

* FEGS = Fly's Eye GLM Simulator, GLM=Geostationary Lightning Mapper

524

525 **The in-Situ Thunderstorm Observer for Radiation Mechanisms (iSTORM)**, is a
526 gamma-ray spectrometer optimized to make sensitive measurements of bright, fast
527 transients in the nuclear gamma-ray band (~ 300 keV to >5 MeV), designed and built by
528 the US Naval Research Laboratory. The iSTORM instrument is a highly segmented
529 array of fast, high-resolution inorganic scintillators. The large total geometric area (157
530 cm^2) provides high sensitivity, while the high segmentation and fast scintillation decay
531 time preserves that large area for bright TGFs, which would paralyze a single detector
532 of equal area. With slightly smaller detector geometric area (157 cm^2 versus 225 cm^2)
533 and a smaller energy range (up to 5 MeV versus 30 MeV) the iSTORM sensitivity and
534 range are slightly smaller than for the BGO. The specification of the iSTORM
535 instrument is listed in Extended Data Table 2.

536

537 **The Fly's Eye Geostationary Lightning Mapper (GLM) Simulator (FEGS)**, is an
538 airborne array of multi-spectral radiometers optimized to measure the optical emission
539 from lightning. These radiometers observe spectral emission from a variety of
540 temperature regimes. The specification of FEGS is given in Extended Data Table 3.
541 With 25 photometers centered at 780 nm FEGS provides images of the 777.4 nm
542 emissions from lightning leaders over a nominal spatial footprint of $10 \times 10 \text{ km}^2$ with a
543 spatial resolution of $2 \times 2 \text{ km}^2$ for cloud top at 15 km. The field-of-view (FOV) of the
544 other photometers is $2 \times 2 \text{ km}^2$ aligned with the center photometer of the 780 nm band.
545 All photometers are sampled with a temporal resolution of $10 \mu\text{s}$.

546

547 **The Electric Field Change Meter (EFCM)** is a two-channel (fast and slow) antenna
548 that measures the derivative of the electric field impulse produced by lightning. The fast
549 channel is designed to isolate the radiative component of the lightning discharge field
550 while the slow channel is optimized to observe the electrostatic field component. The
551 EFCM has multiple sensitivity ranges that are selectable during flight and samples with
552 16-bit resolution. Sample rate and decay time constant for EFCM are given in Extended
553 Data Table 4. The EFCM is a triggered system.

554

555 **The Low Frequency (LF) radio receivers in Mexico and Florida.** The LF magnetic
556 field radio emissions (30–300 kHz) were recorded in Sisal, Mexico (21.16°N latitude
557 and -90.05°E longitude) and in Florida, USA (28.06°N latitude and -80.62°E longitude).
558 The sensors have a flat frequency response from 100 to 200 kHz and a frequency-
559 proportional response from 1 to 100 kHz. These sensors measure 2 orthogonal
560 horizontal magnetic field components and thus also measure the direction of signal
561 arrival. Absolute amplitude calibration was obtained from both laboratory
562 measurements and in-field cross calibration with other magnetic sensors. The signals
563 are sampled at 1 MS/s and GPS timing ensures absolute timing accuracy of better than 1
564 μs . The LF radio measurements are sensitive to electric current pulses with a time scale
565 of $5 \mu\text{s}$ to 1 ms. The noise level varies somewhat in time due to anthropogenic sources,
566 and the sensitivity to a fixed amplitude current pulse varies with distance to the signal
567 source.

568

569 **The Very High Frequency (VHF) Interferometer** system was located at the University
570 of Central Florida (UCF) Townes Institute Science and Technology Experimentation
571 Facility (TISTEF) within the Kennedy Space Center, Florida (28.465163°N , -80.651996°E). VHF radio emissions of 1–160 MHz were recorded at 360 MHz
572 from three sensitive inverted-V VHF antennas arranged in a near right triangle with
573

574 baseline lengths of 24.1, 25.4 and 33.4 meters. Electric field change waveforms
575 obtained from a fast antenna (FA) having ~30 ns risetime and 100 microsecond decay
576 time were simultaneously recorded with the VHF. Trigger lengths were typically 0.75
577 seconds in length with 0.25 seconds of pre-trigger before a triggering broadband VHF
578 pulse.

579

580 **b) Instrument performance of the gamma detectors**

581

582 At 20 km altitude an aircraft can fly directly above the thundercloud and get close (<10
583 km) to the radiation source, so some of the FGFs (and a few TGFs) appeared so bright
584 that some of our gamma-ray detectors saturated.

585

586 As shown in Fig. 1A and pointed out in the main text, the large BGO detector (225 cm^2)
587 was saturated during the eight first pulses, while the smaller LYSO detector (1 cm^2) was
588 not. The reason for this saturation is that the three BGO channels and the one LYSO
589 channel each have a FIFO data buffer of depth 256, and the readout link speed for the 3
590 BGOs and LYSO altogether is around 330 kscdp/s (scdp: science data package of 48
591 bits). The link will loop around and read out one count at a time from every channel
592 only if the FIFO of that channel is not empty. During a bright event of more than 256
593 counts (plus several extra count being read out at the same time) in a short period of
594 time, the FIFO can be full and the following counts are discarded by the firmware until
595 a new count is read out by the link (~75 kscdp/s), this gives the effect of a sudden drop
596 of count rate to around 7.5 counts per 100 us. As seen in the inset of Fig. 1A, this drop
597 is seen during the first eight pulses for BGO, but not in the LYSO data, which due to its
598 much smaller detector area never reaches this count rate.

599

600 The iSTORM data acquisition system is fully independent from that of the BGO.
601 iSTORM employs a commercial CAEN A5202 64-channel front-end electronics board
602 intended for silicon photomultiplier (SiPM) readout of fast scintillators. The front-end
603 board is controlled and read out by a BeagleBone® Black single-board computer
604 (SBC). Data are read out in “Spectroscopy Mode,” in which individual photons are
605 logged by trigger number, time tag, and pulse height, and stored in flash memory.
606 Inspection of the iSTORM data stream shows that the combined front-end board and
607 SBC system is subject to regular busy times, including drop-outs with 2-second and
608 ~0.67-second periods, in which the system is unable to store events for durations of ~1
609 ms to ~10 ms. However, the trigger numbers of the stored events provide a direct
610 measure of the number of triggers dropped during processor and front-end busy times,
611 and it is therefore possible to calculate the total count rate, including triggers lost during
612 these and other busy times. As configured for flights on 6 July and 8 July, iSTORM was
613 particularly susceptible to noise and processor-induced deadtime and thus was not
614 sensitive to the first three FGFs shown in Fig. 2.

615

616 As pointed out in the main text there are a few differences between the BGO data and
617 the iSTORM data in Fig. 2.

618

619 For event #8 deadtime effects in the iSTORM are seen during the 1st, 5th and 6th pulse,
620 while BGO is not seeing the full signal for 7th, 8th and 9th pulse. The deadtime effect of
621 iSTORM is also seen in the 4th pulse of event #6, 12th pulse of #9 and 1st pulse of #24.

622

623 For the event #10 the the BGO was saturated, and the first pulse appears as two separate
624 pulses, while iSTORM shows clearly that this is indeed one large pulse.
625

626 Despite of these differences, the two independent detector systems confirm that the
627 pulses we see are real and cannot be the result of instrumental effects.
628

629 **c) No detectable electrical signals or radio signals from FGFs**

630

631 **EFCM on ER-2**

632 For the 24 FGFs we have EFCM recordings for three of them, LF recordings from
633 Mexico and Florida for all of them and VHF from Florida for the last one (#24).
634

635 Extended Data Fig. 1 shows three FGFs with synchronous EFCM recordings. Since this
636 is a triggered system the EFCM data do not cover the first pulses of the FGF (Extended
637 Data Fig. 1A and 1C). Counts from all three BGO detectors are binned into 100 μ s bins
638 to form the FGF light curves (black lines) with individual pulses clearly visible to the
639 very end of each FGF event. Red lines show electric field variability which was
640 calculated by finding logarithmic mean of the spectral amplitudes for each 100 μ s time
641 bin of the signal, such that the final variability is given by:
642

$$643 \Delta E = 10^M,$$

644

$$645 M = \frac{1}{N} \sum_{k=1}^N \log_{10} S_k,$$

646

647 where S_k are power spectral density amplitudes for the whole frequency range up to 5
648 MHz sampled with a step of 10 kHz (each time bin was 100 μ s).
649

650 Extended Data Fig. 1 clearly shows the absence of a noticeable radio signal during the
651 three FGF events. At the same time, in all events radio recordings show a strong NBE
652 signals (marked with black text and arrows) at about 10 ms after the final pulse of the
653 FGFs (marked with red arrows). Those NBEs start long lasting (hundreds of
654 milliseconds) periods of electromagnetic activity, which can be seen in each red curve
655 after the NBE.
656

657 **LF from Mexico and Florida**

658 Performance details for these sensors are described in Section 2a. Signals during all 24
659 FGFs from the campaign were recorded by multiple sensors. The closest sensors were
660 either Sisal, Mexico, or Melbourne, Florida. In all cases, there was no detectable signal
661 above the noise floor during the time of the FGFs that originated near the FGF location.
662

663 The noise floor of the recorded signals enables us to establish an upper bound on the
664 strength of any radio emissions associated with the FGFs. In the Extended Data Fig. 2
665 we show instantaneous LF magnetic field power for the horizontal magnetic field
666 component maximized for the direction to the FGF location. Lightning pulses that

667 arrive from directions deviating by more than 20° in azimuth from the FGF location are
668 masked out because these cannot be associated with the FGF.

669
670 To create a meaningful measure of sensitivity, we determine the expected amplitude of
671 sources with known peak current values by establishing a correlation between the peak
672 currents reported by the National Lightning Detection Network (NLDN) and the peak
673 fields measured by the LF sensor for a source of known distance away. As an
674 illustration, when examining the FGF located 75 km away from the sensor, we measure
675 the peak LF fields of NLDN-reported events measured at the same distance (75-76 km)
676 from the source. For a specific peak current value, a range of peak fields that span
677 approximately a factor of 2 are found, and we utilize the median value as a
678 representative measure for the equivalent field of that peak current.

679
680 Extended Data Fig. 2 shows the measured LF signal power during the time window of
681 two FGF events. The first is the event analyzed in the main text from 2023/07/08
682 05:01:12 UTC (Extended Data Fig. 2A). The closest LF signal was measured in Sisal at
683 922 km distance. The background noise level shows that any FGF-associated radio
684 signal would have to be from a source smaller than approximately 1 kA equivalent peak
685 current. The second event is from 2023/07/29 21:03:19 UTC (Extended Data Fig. 2B).
686 The closest LF signal was measured in Melbourne at 75 km distance. This is the FGF
687 with the shortest distance to one of our LF sensors and thus the highest sensitivity to
688 small signals. The background noise level shows that any FGF-associated radio signal
689 would have to be from a source at least 10 times smaller than 1 kA peak current.

690
691 These measurements establish a strong upper bound on any possible LF radio emissions
692 associated with FGFs. They confirm that the FGFs initiate and develop in the absence
693 of any typical lightning flash processes.

694
695 **VHF and FA from Florida**
696 VHF source azimuths as mapped by the interferometer within a 200-millisecond interval around
697 the time of the FGF are shown in Extended Data Fig. 3A with raw data superimposed and the
698 FGF shown in Extended Data Fig. 3B. The signals seen at the two azimuth angles are ~ 30 km
699 away from the receiver, which means that the signals coming from $\sim 320^\circ$ azimuth are ~ 5 km
700 horizontal distance from the ER-2 location. There is activity from a storm about 40 km
701 south of the ER-2 location ($\sim 250^\circ$ azimuth), but no VHF sources are detected from the storm
702 near the ER-2 ($\sim 320^\circ$ azimuth), during the time of the FGF, consistent with the interferometer's
703 FA waveform being silent, as well as the EFCM (Extended Data Fig. 1, lower panel) and LF
704 (Extended Data Fig. 2B) measurements for this event. An NBE and subsequent IC flash from
705 that storm is detected 14.5 ms after the last FGF pulse.

706
707 **d) No detectable optical signals from FGFs**
708
709 We have optical measurements by the FEGS, on board the aircraft for 22 of the of the
710 24 FGFs. The channels that are most sensitive to lightning activity, are the

711 25 photometers centered at 780 nm and one photometer centered at 340 nm. These two
712 channels measure the 777.4 nm emission line from atomic Oxygen (OI) formed by
713 disassociated molecular Oxygen in the hot leader channel, and the 337.1 nm emission
714 line from and molecular Nitrogen (N₂P) from colder streamer ionization waves.

715

716 Extended Data Fig. 4 shows all the FGFs and the accumulated optical signals from
717 777.4 nm emissions (red) and 337.1 nm emissions for 22 of the events. The negative
718 slopes that are seen in some of the panels are due to undershoot in the FEGS signals
719 after pulses. It can be seen that all the FGFs, except events #20 and #21 where the
720 FEGS instrument was not working, are followed by continuous lightning activity.

721

722 All the panels, except two, show that there is no optical activity within the FOV of the
723 FEGS during the FGFs. In event #1 there are a few small optical pulses (seen as steps)
724 which are not correlated in time with the pulses of the FGF (up to 10 ms delayed) and
725 are likely from a different location than the FGF. The weak optical signals in event #5
726 that start before the FGF do not show any pulsed features and are most likely unrelated
727 to the FGF.

728

729 The FOV of FEGS is 10 km x 10 km (5-7 km to the corners/sides for a cloud top at 15
730 km), but can see scattered light from at least 10 km from aircraft foot-point. Although
731 the sensitivity of BGO falls off drastically from foot-point to 20 km horizontal distance
732 (4 orders of magnitude)³², strong signals from 20 km will still appear as weak signals
733 above the noise level. However, more than half of the FGFs have intensities that
734 indicate a source less than 5 km from foot-point and well within the FEGS FOV, and we
735 do not see any optical signals for any of them. See also Methods 2e where the radial
736 distance for two of these events are estimated by modelling.

737

738 For the weaker FGFs (9 total) we cannot exclude that the gamma source is more than 10
739 km away and therefore any light associated with them would not be seen by FEGS, but
740 it is quite unlikely that this should occur for all of them.

741

742 e) Spectral characteristics and fluence estimates

743

744 In Extended Data Fig. 5 the spectral characteristics of two of the FGFs are shown. From
745 the BGO instrument, which covers energies from 300 keV to >30 MeV, these two FGFs
746 are among the brightest we observed and have sufficient count statistics to identify the
747 shape of their energy spectrum and make an estimate of the fluence at source.

748

749 All the observed spectra are expected to come from the Relativistic Runaway Electron
750 Avalanche (RREA) process. To assess if a typical RREA spectrum is detected, we used
751 the GEANT4 software³⁵, that enabled us to simulate photon, electron, and positron
752 propagation in any medium (here: the atmosphere, the detectors and surrounding
753 structures). We tested a classical RREA photon spectrum of $1/E * \exp(-E/7.3 \text{ MeV})$ up

754 to 40 MeV at source, and a simple power law 1/E, which would be just an enhancement
755 of the background spectrum, termed Modification of Spectrum (MOS)³⁶.
756

757 To perform the spectral analysis and find the best model fits, the following steps were
758 performed; 1) Propagation, scattering and absorption of gamma photons in the
759 atmosphere, as well as the production of secondary electrons and positrons, from 15 km
760 altitude to the aircraft altitude at 20 km. 2) Energy Response Matrix of the BGO
761 instrument, including scattering in the aircraft body, housing of the instrument and the
762 other instruments in the aircraft pod located in the wing of the aircraft. 3) Maximum
763 likelihood analysis to find the best parameter fits, using the same method as in ref.³⁷
764 based on the statistical approach presented by ref.³⁸
765

766 The Extended Data Fig. 5 shows spectral fits for A) Event #2: 2023-07-08 at
767 05:01:12.451 UT. B) Event #9: 2023-07-24 at 06:56:07.270 UT. In both cases all the
768 pulses, 17 (Fig. 1) and 16 (Fig. 3), respectively, are included. For both cases, the RREA
769 model is a significantly better fit compared to the 1/E power law. This is shown by the
770 Negative Log Likelihood values (NLL), where lower value means better fit. The NLL
771 values for the model fits are listed in Extended Data Table 6. This demonstrates that a
772 RREA process is the most likely explanation of the observed spectra. The spectral fits
773 also give us the best fit radial distances (i.e. horizontal distance between the FGF source
774 location and the aircraft). For these two FGFs the best radial distance is 3 km and 5 km,
775 respectively, and gives support to our claim that the source of these bright FGFs is close
776 to the aircraft foot-point. This estimate is for a source altitude at 15 km.
777

778 Combining all pulses for each event, we can estimate the number of source photons
779 (above 400 keV) to be 1.5×10^{16} (event #2) and 7×10^{16} (event #9), assuming a source
780 altitude at 15 km, which is used here as a reference altitude to compare with ASIM
781 detections from the same assumed altitude. For event #9 half of these photons are from
782 the first 50 ms long pulse, so the total number of photons for all the short 1-2 ms long
783 pulses is on the order of 10^{16} , which would give about 10^{15} photons in each pulse at 15
784 km. We emphasize that these estimates are for the pulses in two of the brightest FGFs
785 we observe. The majority of FGFs has lower fluence than these two. Of current
786 spaceborne gamma detectors ASIM has the highest sensitivity and can identify gamma
787 events with $>5.6 \times 10^{15}$ gamma photons (Table 1) from a source at 15 km within its
788 trigger windows of 300μs, 1 ms, 3 ms or 20 ms. Pulses with $\sim 10^{15}$ photons are just
789 below the detection threshold of ASIM and are consistent with the non-detection of
790 FGFs by any of the current spaceborne detectors (see Table 1 and Methods 1f).
791

792 **f) Flux values for glows, FGFs and TGFs at 20 km from measurements**

793 Here we explain how the flux values given in Table 1 for glows, FGFs and TGFs at 20
794 km altitude are obtained.
795

796

797 A glow is identified when the background of 2000 cnts/s increases by 25% (500 cnts/s),
798 which then defines the lower flux limit for glows. The most intense glow we see is \sim 10
799 times the background (20 000 cnts/s). With a detector area of 225 cm² we get a range of
800 2 – 90 (cm² s)⁻¹.

801

802 We have several FGFs where the BGO was saturated, but LYSO was not. This is the
803 case for FGF #2, #8, #14 and #21, which are the four brightest FGFs we observe. Using
804 the light-curve of the unsaturated LYSO we can estimate what the peak flux in BGO
805 should have been. These estimates are listed in Extended Data Table 7, and the largest
806 estimate we find is for 1st pulse in #21, where the measured flux should be increased to
807 1358 cnts/100 μ s (a factor of 3.5). The lowest maximum peak flux we observe during a
808 FGF is the 3rd pulse of #10 (\sim 40 cnts/ms). With a detector area of 225 cm² this gives us
809 a range of $1.8 \times 10^2 - 6.0 \times 10^4$ (cm² s)⁻¹.

810

811 For TGFs we will give the flux range based on the ASIM measurements mapped down
812 to 20 km altitude, assuming production altitude at 15 km. The weakest TGF that can be
813 identified in the ASIM data is \sim 10 cnts/ms and the brightest is \sim 1000 cnts/500 μ s. The
814 ASIM MXGS HED detector area is \sim 900 cm². Combining the absorption from 20 km to
815 400 km (factor of 8 obtained from GEANT simulation) and the 1/r² effect (factor of
816 6400), the total scaling factor between 400 km and 20 km is \sim 50 000. Taking both the
817 detector area and the total scaling factor into account we get a range of $5.6 \times 10^5 - 10^8$
818 (cm² s)⁻¹ for ASIM TGFs mapped down to 20 km. Only a few (3-4) of the 96 TGFs
819 seen during the ALOFT campaign had fluxes above this lower limit and could have
820 been seen from space. The brightest peak flux of a single pulse in the FGFs we observed
821 (1st pulse of #21) is just below the lower threshold and would probably not been
822 identified in data from any current spaceborne detectors.

823

824

825

826

827

828

829

830

831

832

833

834

835

836

837

838

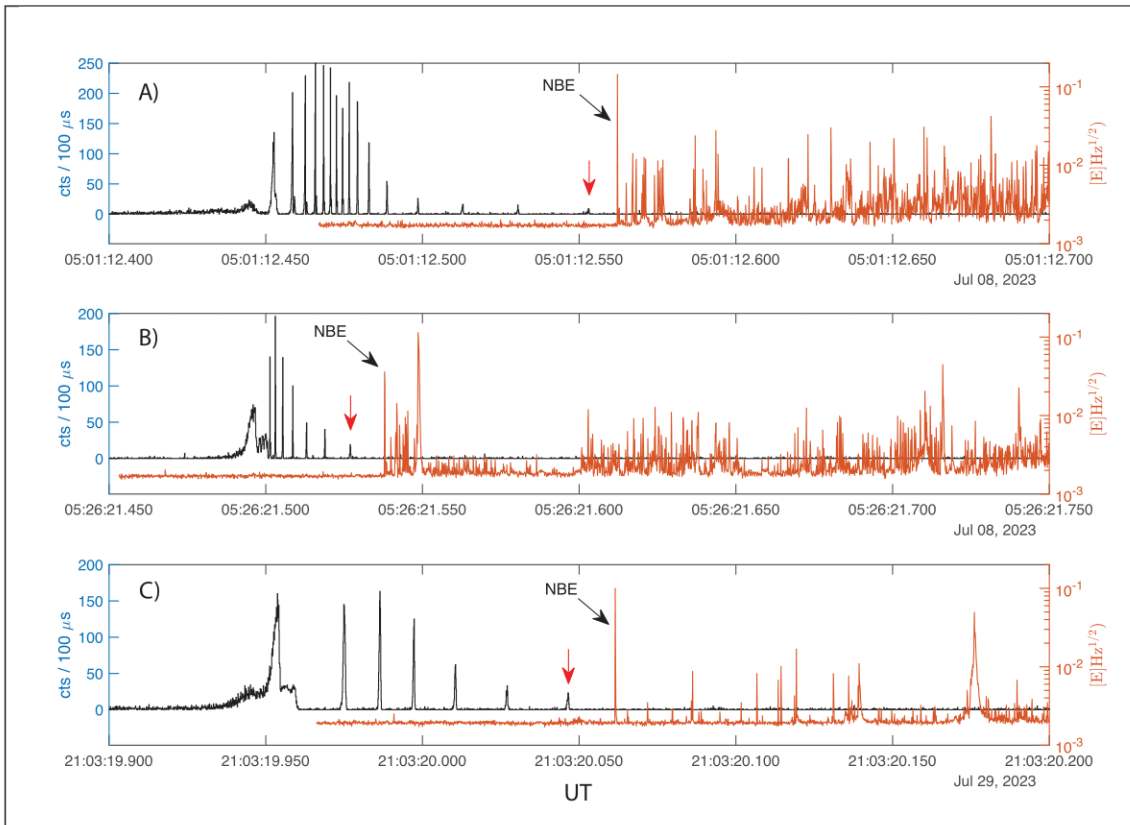
839

840

841

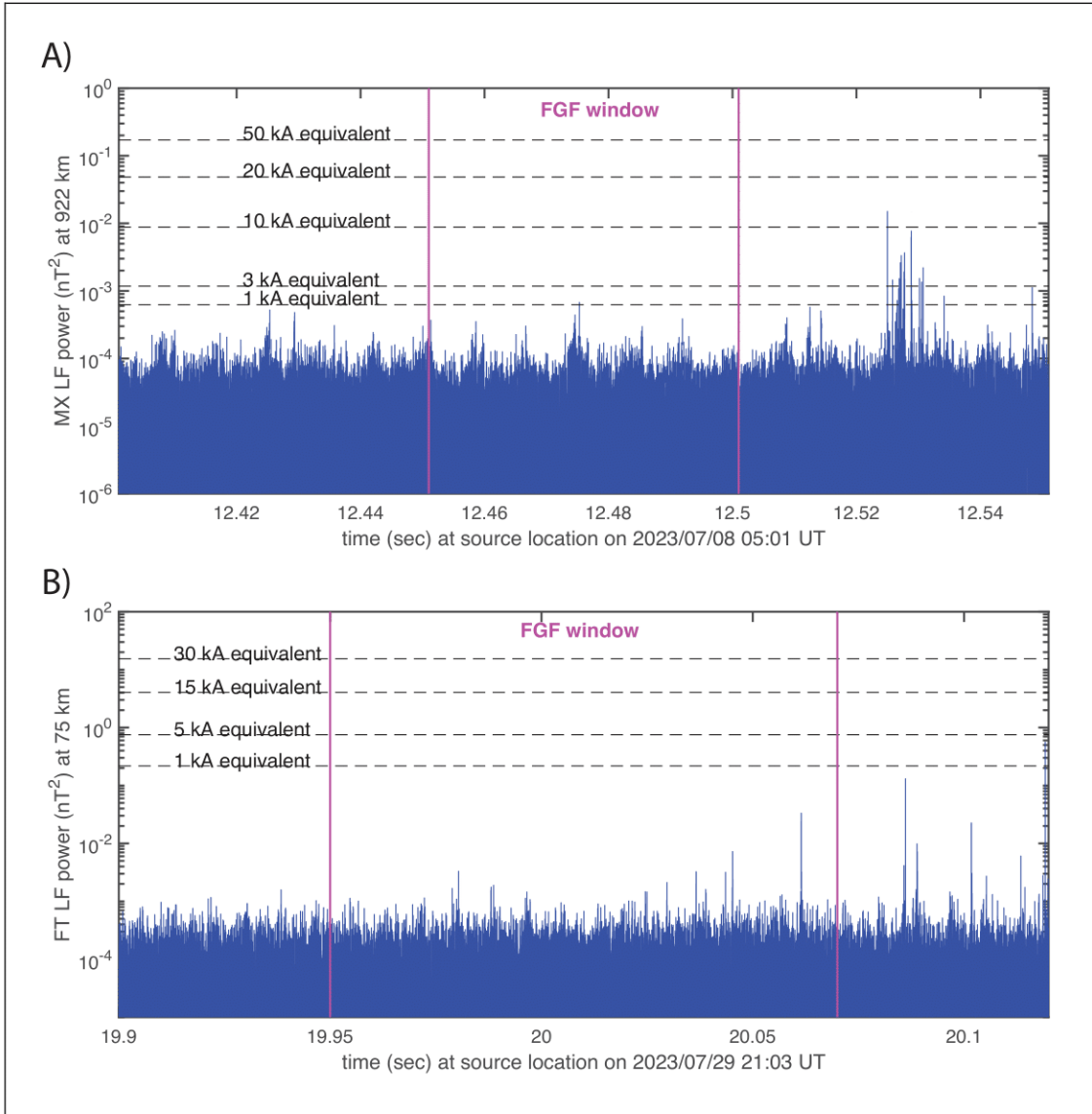
842

843
844
845
846
847
848
849
850
851
852
853
854
855 EXTENDED DATA FIGURES AND TABLES
856
857
858
859



860
861 **Extended Data Fig. 1. Three FGF events with EFCM recordings.** Black lines show FGF light
862 curves of the FGFs, while red lines represent electric field variability as recorded by EFCM. The
863 last pulse of the FGF is marked with a red arrow and the following NBE with a black arrow.
864
865
866
867
868
869

870
871
872
873
874
875
876
877
878
879



880
881 **Extended Data Fig. 2. LF signal power during the time window of two FGF events.** Overlaid
882 are the data-derived peak power of lightning pulses at the observed distance for a range of peak
883 currents. For the 2023/07/08 05:01:12 UTC FGF (panel A), the noise level and 922 km distance
884 imply that any current pulses associated with the FGF must be lower than 1 kA equivalent. For
885 the 2023/07/29 21:03:19 UTC FGF (panel B), the noise level and much shorter 75 km distance
886 that any current pulses associated with the FGF must be at least 10 times smaller than 1 kA.
887